






Elastic criterion for shear-banding instability in amorphous solidsX. J. Wang ^{1,2,3} Y. Z. Lu ^{2,*} X. Lu,² J. T. Huo ^{4,†} Y. J. Wang ^{1,3} W. H. Wang,⁵ L. H. Dai,^{1,3} and M. Q. Jiang ^{1,3,‡}¹State Key Laboratory of Nonlinear Mechanics, Institute of Mechanics, Chinese Academy of Sciences, Beijing 100190, People's Republic of China²School of Materials Science and Engineering, Dalian Jiaotong University, Dalian 116028, People's Republic of China³School of Engineering Science, University of Chinese Academy of Sciences, Beijing 100049, People's Republic of China⁴Ningbo Institute of Materials Technology and Engineering, Chinese Academy of Sciences, Ningbo 315201, People's Republic of China⁵Institute of Physics, Chinese Academy of Sciences, Beijing 100190, People's Republic of China

(Received 16 November 2021; revised 21 February 2022; accepted 5 April 2022; published 25 April 2022)

In amorphous solids, plastic flow is prone to localization into shear bands via an avalanche of shear-transformation (ST) rearrangements of constituent atoms or particles. However, such banding instability still remains a lack of direct experimental evidence. Using a real 3D colloidal glass under shear as proof of principle, we study STs' avalanches into shear banding that is controlled by strain rates. We demonstrate that, accompanying the emergent shear banding, the elastic response fields of the system, typical of a quadrupole for shear and a centrosymmetry for dilatation, lose the Eshelby-type spatial symmetry; instead, a strong correlation appears preferentially along the banding direction. By quantifying the fields' spatial decay, we identify an elastic criterion for the shear-banding instability, that is, the strongly correlated length of dilatation is smaller than the full length of shear correlation. Specifically, ST-induced free volume has to be confined within the elastic shear domain of ST so that those STs can self-organize to trigger shear banding. This physical picture is directly visualized by tracing the real-space evolution of local dilatation and ST particles. The present work unites the two classical mechanisms: free volume and STs, for the fundamental understanding of shear banding in amorphous solids.

DOI: [10.1103/PhysRevE.105.045003](https://doi.org/10.1103/PhysRevE.105.045003)**I. INTRODUCTION**

Shear banding describes the plastic or flow instability that localizes large shear strain into a relatively narrow band, which is commonly observed in nature and technology [1–6]. For amorphous solids (e.g., metallic glasses, granular materials, colloidal glasses, etc.), shear-banding instability often easily occurs to be the culprit behind their unpredictable and often catastrophic failure. In past decades, the physical process of how a shear band emerges from disordered structure has aroused a great deal of interest and meanwhile much controversy. Nevertheless, there is a general consensus that shear bands in amorphous solids are structurally dilatant in essence [7–15], pointing to the so-called Reynolds dilatancy [16].

In amorphous solids, basic units of plastic events have been identified as shear transformations (STs), i.e., localized irreversible rearrangements of small groups of atoms or particles. It has been widely recognized that dynamic STs operate transiently, but giving rise spatially to nonlocal Eshelby-type shear fields around them. Via such elastic interactions, a series of STs can be successively activated, like avalanches, and ultimately develop into system-spanning shear bands with

characteristic thicknesses. However, this universal picture is evidenced mainly by indirect experiments [17–19], numerical simulations [12,14,20–23], and theoretical modeling [17,24–27]. Firsthand experimental proof is very rare [28], especially in thermal particle systems. On the other hand, the dilatancy of shear banding is mostly reflected by postmortem probe into density or volume within bands. In fact, local creation of free volume is not only a consequence of STs, but also a prerequisite for STs' initiation [12,29,30]. A few works [10,13] have probed a critical dilatation needed for the shear-banding initiation. Nevertheless, the crucial role of STs' dilatancy in shear banding is highly underestimated or even totally neglected. Up to now, there has not yet been a direct experiment to elucidate the emergence of shear banding from *the causality between elastic shear and dilatation responses of STs*. Specifically, what are their respective roles of STs' shear and dilatancy in shear-banding instability? Or, in what condition are STs responsible for shear banding (or self-assembly of avalanched STs) in amorphous solids?

In this paper, we answer these challenging questions with resorting to a real 3D silica-particle colloidal glass under simple shear. This amorphous solid displays the homogeneous deformation at low strain rates and the shear-banded inhomogeneous flow at strain rates higher than the inverse structural relaxation time. We calculate the spatial autocorrelation of both shear strain and free volume at the particle level, which characterizes with fidelity the elastic shear and dilatation fields induced by STs, respectively. It is found that

*luyz@djtu.edu.cn

†huojuntao@nimte.ac.cn

‡mqjiang@imech.ac.cn

both fields can be resolved into a strongly correlated core and a weakly correlated outside region, but showing very differing rate dependence. The spatial-decay analyses of these elastic fields reveal that the shear banding emerges if and only if the core size of strongly correlated dilatation is smaller than the full correlation length of shear distortion. This elastic criterion implies that only these STs, whose induced free volume is confined within their elastic shear field, have the chance to self-organize into a shear band; otherwise they will isotropically nucleate in space and ultimately contribute to homogeneous deformation. The two modes are further verified by tracing the evolution of local dilatation and dilatation-mediated STs in this real glass.

II. MATERIALS AND METHODS

A prototypical colloidal glass was prepared by using the hard-sphere silica particles with a polydispersity smaller than 3.5% and the diameter $2R = 1.55 \mu\text{m}$. The silica particles were suspended in a mixture (solvent) of deionized water (30% vol.), dimethylsulfoxide (69% vol.), and fluorescein-NaOH solution (1% vol.). The density difference $\Delta\rho$ between particle and solvent was $\sim 0.9 \text{ g/cm}^3$, which induced the spontaneous sedimentation of particles in the solvent due to gravity. Under the gravitational sedimentation, the deposition flux of particles is the control parameter corresponding to the quench rate for the glass formation. The dimensionless particle flux is defined as $\phi_0\text{Pe}$, where $\phi_0 \approx 0.04$ is an initial volume fraction of particles and Pe is the Péclet number accounting for the ratio of the rate of the sedimentation to that of diffusion. The calculated Péclet number $\text{Pe} = \Delta\rho g R^4 / (k_B T) \approx 0.8$, where g is the gravity constant, k_B the Boltzmann constant, and T the room temperature. Jensen *et al.* [31] extensively studied the effect of the deposition flux $\phi_0\text{Pe}$ on the resulting colloidal structures, and found that colloidal glasses can be formed above $\phi_0\text{Pe} \approx 0.02$. In the present work, the deposition flux $\phi_0\text{Pe} \approx 0.032$, which ensured the formation of the colloidal glass with the volume fraction of 0.61 ± 0.1 [32]. The long-range disordered structure of the as-prepared colloidal glass was confirmed by its radial distribution function (RDF), as shown in Fig. 1(a) where the inset shows a typical cross section of the glassy structure. The structural relaxation time of the as-prepared glass was measured to $\tau \sim 2 \times 10^4 \text{ s}$ from the mean-square displacement (MSD) of particles with the time [11,32–35], as shown in Fig. 1(b). The MSD at short time exhibits the vibrational plateau. This indicates that the present colloidal glass is a thermal particle system and thus representative of a broad range of amorphous solids.

The colloidal glass was sheared in a cell between a transmission electron microscope (TEM) grid and a fixed coverslip with the shear gap of higher than $200 \mu\text{m}$. A schematic of the shear cell is shown in Supplemental Material, Fig. S1 [32]. Through a hollow post, a piezoelectric translation stage was used to move the TEM grid, thus applying a simple-shear loading along the y direction at a constant strain rate. This shear technique was originally developed by the Spaepen and Weitz group [33,36]. Here, four groups of shear strain-controlled experiments were performed and the applied strain rates $\dot{\gamma}$ were, respectively, set to be 1.0×10^{-5} , 4.0×10^{-5} ,

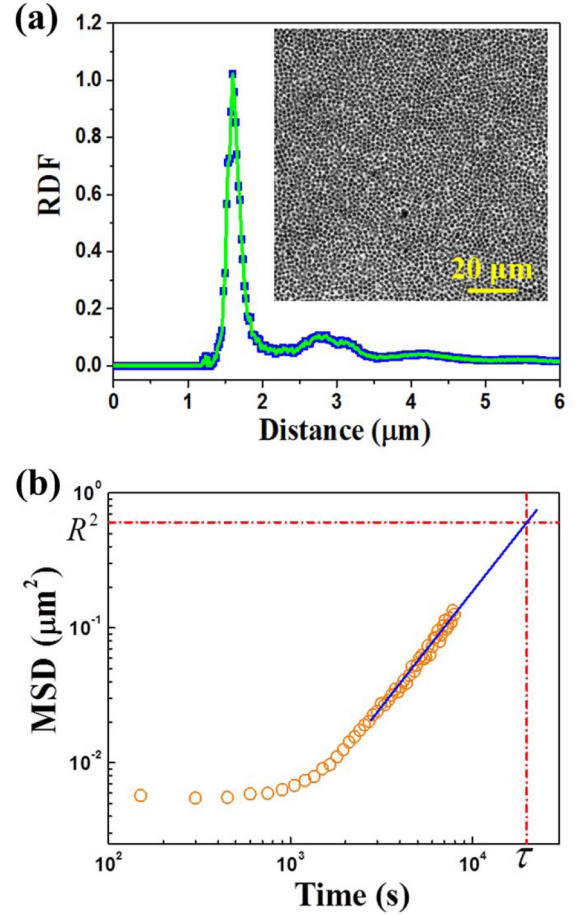


FIG. 1. (a) RDF of the as-prepared colloidal glass. Inset: a typical cross section of the glassy structure. (b) MSD of all particles vs the time.

8.0×10^{-5} , and $1.2 \times 10^{-4} \text{ s}^{-1}$. The first two $\dot{\gamma} < \tau^{-1}$, while the last two $\dot{\gamma} > \tau^{-1}$. In the z direction, a high-speed confocal microscopy was used to visualize about 74 000 particles in a $77 \times 77 \times 40 - \mu\text{m}^3$ observation volume that was far away from the sample boundaries during shear. The deformation behaviors observed from this 3D window ruled out the possibility of any finite-size or boundary effect. The trajectories of individual particles for the shear duration were carefully tracked by acquiring 3D image stacks every 200 s (time step). Before each shear loading, the colloidal glass was restored to its initial state through sufficiently long-time relaxation, which is evidenced in Figs. S2 and S3 [32].

The particle-level, local shear strain ε_{ij} can be calculated from the relative motion of a particle with respect to its nearest neighbors, based on the D_{\min}^2 concept of Falk and Langer [37]. We first define the nearest-neighbor displacement vector $\mathbf{d}_n(t) = \mathbf{r}(t) - \mathbf{r}_n(t)$, where $\mathbf{r}(t)$ is the particle position at arbitrary time t , and n is the number of the nearest neighbors that is determined according to the RDF [Fig. 1(a)]. Then, the best affine deformation gradient tensor $\mathbf{\Gamma}$ that transforms the change of $\mathbf{d}_n(t)$ over the time interval Δt can be found by minimizing $D^2 = \sum_n [\mathbf{d}_n(t + \Delta t) - \mathbf{\Gamma} \times \mathbf{d}_n(t)]^2$. The ε_{ij} is calculated as the symmetric part of $\mathbf{\Gamma}$, where the indices i

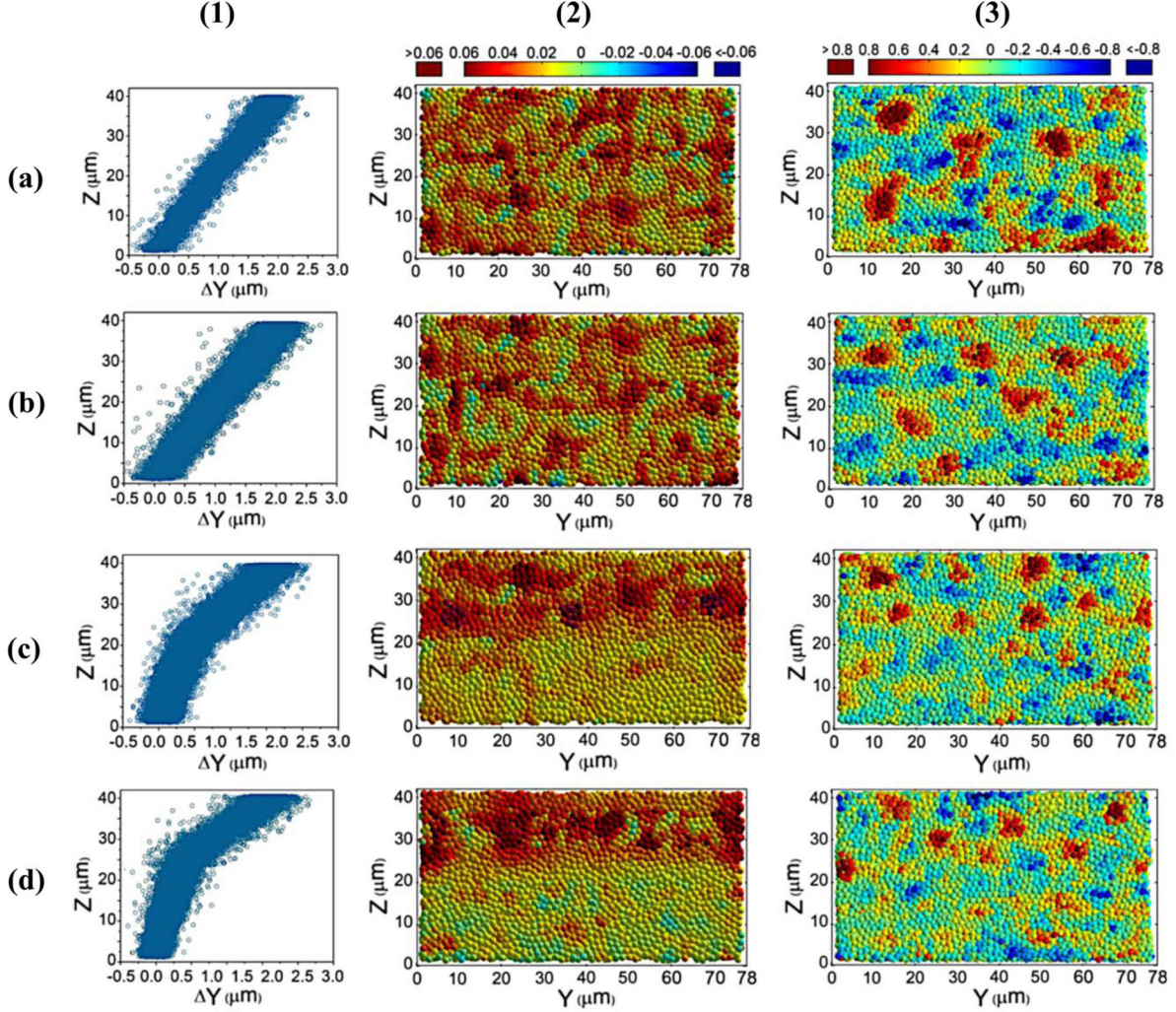


FIG. 2. Strain-rate dependent deformation modes of the colloidal glass sheared to the same macroscopic shear strain of 0.048. (a)–(d) Strain rates: $\dot{\gamma} = 1.0 \times 10^{-5}$, 4.0×10^{-5} , 8.0×10^{-5} , and $1.2 \times 10^{-4} \text{ s}^{-1}$. Column (1) shows the the deformation displacement profiles $\Delta y(z)$ of particles. Columns (2) and (3) are the $6\text{-}\mu\text{m}$ -thick y - z section (centered at $x = 24 \mu\text{m}$) reconstructions showing the spatial distribution of local shear strain ε_{yz} and local dilatation ξ of particles, respectively, where the color denotes the cumulative ε_{yz} or ξ magnitude with the reference zero-strain state.

and $j \in x, y$, and z . In the present simple-shear case, only ε_{yz} survives and other components are negligibly small.

The particle-level, local dilatation ξ was originally defined by some of us [29]. For a particle with a volume of v_0 , its ξ can be calculated as $\xi = (\Delta v_f / v_0) / |\Delta \varepsilon_{yz}|$ that evaluates the increase Δv_f of local free volume induced by an increment $\Delta \varepsilon_{yz}$ of local shear strain during one time step (200 s). The local free volume v_f is calculated according to previous work [29,38–40]. A 2D schematic that illustrates the v_f calculation is provided in Fig. S4 [32]. First, we construct the Voronoi polyhedra for all particles according to the standard tessellation method [41]. The solid-blue lines are the Voronoi faces that enclose Voronoi polyhedra. Then, we move the Voronoi faces inwards by a distance of the particle radius R , as indicated by the black arrows. The remaining volume surrounded by the dotted-red lines gives an estimation of v_f of the central particle. Within this volume v_f , the center of a particle could move freely, but its surface never crosses the Voronoi faces that surround it.

III. RESULTS AND DISCUSSION

A. Rate-modulated deformation modes

Figure 2 shows the deformation modes of the colloidal glasses that were sheared to the same macroscopic strain $\gamma = 0.048$, but under different strain rates (a)–(d): $\dot{\gamma} = 1.0 \times 10^{-5}$, 4.0×10^{-5} , 8.0×10^{-5} , and $1.2 \times 10^{-4} \text{ s}^{-1}$. Column (1) presents the cumulative displacement profiles $\Delta y(z)$ of all particles. We observe that the deformation at $\dot{\gamma} < \tau^{-1}$ is spatially homogeneous with a singly linear profile. At $\dot{\gamma} > \tau^{-1}$, however, the deformation separates into two coexisting bands with piecewise linear profiles. The shear deformation is mainly localized into the top band that undergoes the higher strain and strain rate than externally incurred. The higher the strain rate is, the more pronounced the shear localization becomes. It is noteworthy that the transient shear banding occurring here is thermally activated, but driven by mechanical loadings. This mechanism is consistent with shear banding in metallic glasses, and the latter is solidly evidenced

by the temperature-dependent shear-band dynamics [42–44]. By contrast, the bottom band attached to the fixed boundary shows a slowing-down deformation. The strain-rate dependent deformation mode transition observed here is consistent with that previously reported in other amorphous systems [11,15,45–47]. It is noted that the applied strain rates are in the vicinity of τ^{-1} , where the shear banding emerges from the homogeneous deformation. However, at very high rates far above τ^{-1} , whether this colloidal glass enters a steady-state shear banding [48] or fails with a brittle manner [46] needs further studies.

The rate-dependent deformation modes can be further indicated by the spatial distribution of local shear strain ε_{yz} of particles, as shown in column (2) of Fig. 2. At $\dot{\gamma} < \tau^{-1}$, the ε_{yz} distribution is homogeneously fluctuated throughout the sample. At $\dot{\gamma} > \tau^{-1}$, the fluctuation becomes heterogeneous, and high- ε_{yz} particles are concentrated in the top shear band, contributing to its macroscopic speed-up deformation. Column (3) shows the spatial distribution of local dilatation ξ of particles, also with an obvious rate effect. At $\dot{\gamma} < \tau^{-1}$, there exist many positive- and negative- ξ clusters (resembling liquidlike and solidlike regions), both homogeneously distributed with each other. This is a sharp contrast to the ε_{yz} distribution whose values are mostly positive. Therefore, the system-averaged shear strain should be larger than the averaged dilatation, which corresponds to the stress analyses by Derlet *et al.* [49]. The positive- and negative- ξ clusters observed here are also consistent with the dilating and contracting plastic events found numerically in granular matter [50]. With increasing $\dot{\gamma}$, these positive- ξ clusters become smaller sizes, and tend to coalesce in the top band. Nevertheless, some negative- ξ clusters can be also observed in the band region. These observations qualitatively agree well with the reported density or volume fluctuation in shear bands [11,12,14,17,51], pointing to the dilatancy of shear banding in amorphous solids. We also find that particles with higher ξ are spatially close to those that underwent larger ε_{yz} , reminiscent of the experimental finding that larger shear strain drives higher volumetric dilatation within shear bands [52,53].

B. Elastic correlation fields

We calculate the spatial correlation of local ε_{yz} or ξ of particles, for exploring the system's elastic responses to the observed rate-induced transition of deformation modes. The normalized autocorrelation function for $\vartheta = \varepsilon_{yz}$ or ξ in 3D space is defined as

$$C_{\vartheta}(\Delta\mathbf{r}) = \frac{\langle \vartheta(\mathbf{r} + \Delta\mathbf{r})\vartheta(\mathbf{r}) \rangle - \langle \vartheta(\mathbf{r}) \rangle^2}{\langle \vartheta^2(\mathbf{r}) \rangle - \langle \vartheta(\mathbf{r}) \rangle^2}, \quad (1)$$

where $\Delta\mathbf{r}$ are the distance vectors between arbitrary two particles, and the angular brackets denote the average over all particles. The angle-resolved $C_{\varepsilon_{yz}}(\Delta\mathbf{r})$ fields for the cumulative ε_{yz} after $\gamma = 0.048$ at the four strain rates are calculated in Fig. 3, where the characteristic y - z plane views are shown as usual. It is clear to see that the elastic shear fields consist of a strongly correlated local core and a correlation-decayed nonlocal outfield. The shape of the cores is close to a circle (a sphere in 3D), and their sizes seem to be unchanged with varied strain rates. But, the outfields are highly rate dependent.

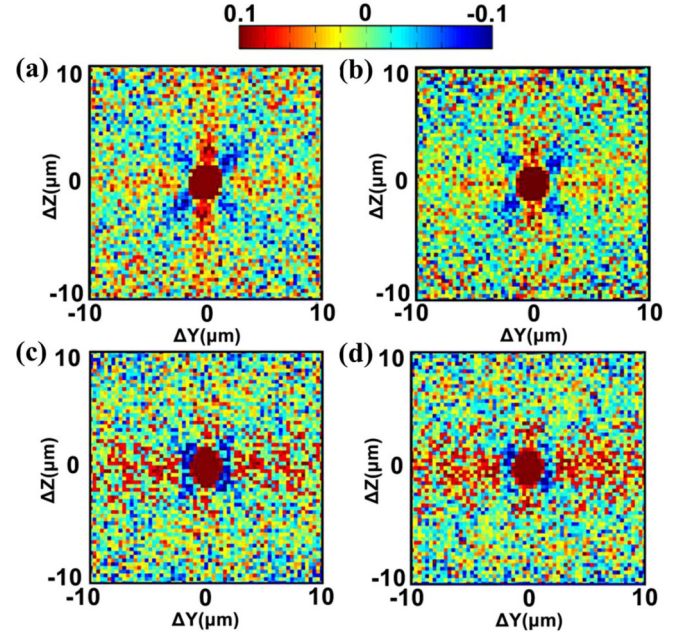


FIG. 3. The y - z plane views of the 3D spatial autocorrelation function of the local shear strain ε_{yz} of particles. (a)–(d) Strain rates: $\dot{\gamma} = 1.0 \times 10^{-5}$, 4.0×10^{-5} , 8.0×10^{-5} , and $1.2 \times 10^{-4} \text{ s}^{-1}$.

At $\dot{\gamma} < \tau^{-1}$ [Figs. 3(a) and 3(b)], characteristic quadrupole patterns are reproduced, which signify that Eshelby-type STs are active in the sheared glass. These STs can be approximately regarded as spherical Eshelby inclusions embedded in infinite isotropic elastic medium [54,55]. Similar Eshelby-type elastic shear signals have been widely observed in other colloidal glasses [11,34,36], thermal or athermal amorphous solids [30,56], granular solids [23,28], and even supercooled liquids under shear [57]. When the glass is sheared at $\dot{\gamma} > \tau^{-1}$ [Figs. 3(c) and 3(d)], the outfield loses the fourfold azimuthal symmetry, where a strong correlation preferentially appears along the shear y direction. This provides an elastic shear signal of the shear banding (or avalanched STs), as pointed out by Chikkadi *et al.* [11,34].

Figure 4 shows the y - z plane views of the dilatation correlation fields $C_{\xi}(\Delta\mathbf{r})$ of particles under the four strain rates. Again, the $C_{\xi}(\Delta\mathbf{r})$ full field consists of a strongly correlated core and an outside region with the correlation decay. But, very different from the shear cases (Fig. 3), both core and outfield of $C_{\xi}(\Delta\mathbf{r})$ highly depend on the strain rates. At $\dot{\gamma} < \tau^{-1}$ [Figs. 4(a) and 4(b)], the cores are nearly the circular (spherical in 3D) shape. The outfields display a unique centrosymmetric feature, instead of the shearlike quadrupole. As strain rates increase to the banding range ($\dot{\gamma} > \tau^{-1}$), the spherical cores gradually become an ellipsoid with its long axis inclined to the shear y direction and meanwhile their sizes decrease [Figs. 4(c) and 4(d)]. The shear banding also entails the symmetry breaking of the dilatation outfield that shows an enhanced correlation along the y direction. *This is an experimental presentation of Eshelby-type dilatation transformations (DTs) in amorphous solids, and the dilatation signal of both isolated STs and shear banding (or avalanched STs) is a refreshing outcome. We must point out that the DTs*

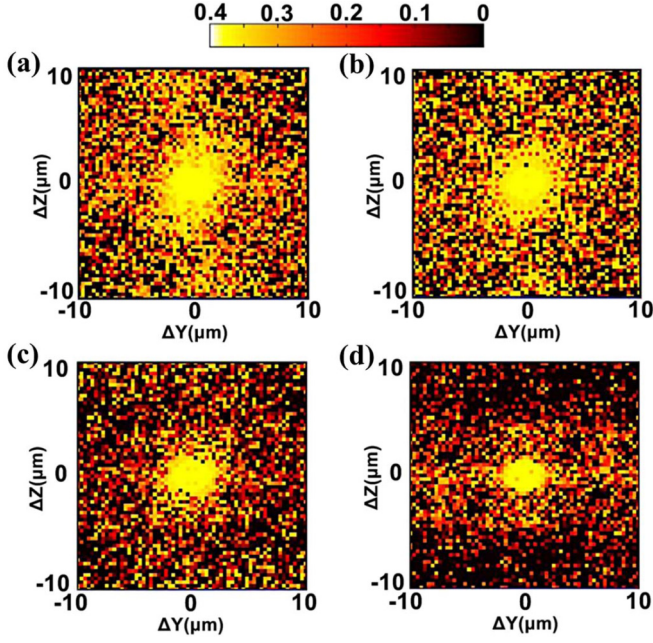


FIG. 4. The y - z plane views of the 3D spatial autocorrelation function of the local dilatation ξ of particles. (a)–(d) Strain rates: $\dot{\gamma} = 1.0 \times 10^{-5}$, 4.0×10^{-5} , 8.0×10^{-5} , and $1.2 \times 10^{-4} \text{ s}^{-1}$.

here are induced by STs rather than directly by pure dilatation sources.

C. Spatial correlation lengths

We quantitatively analyze the spatial decay of the system's shear and dilatation fields (Figs. 3 and 4) to extract characteristic correlation lengths related to STs. In 3D space, the angle-averaged shear $C_{\varepsilon_{yz}}(\Delta\mathbf{r})$ or dilatation $C_{\xi}(\Delta\mathbf{r})$ correlation is calculated as a function of any possible interparticle distance $|\Delta\mathbf{r}|$ that is not below the first-neighbor shell. As shown in Fig. 5(a), the averaged shear correlation at each strain rate exhibits the two-stage decay: an exponential decay in cores followed by a power-law decay in outfields. The two-stage decay is consistent with the Eshelby-inclusion theory [30,36,49,54,55], although elastic fields for inclusions or cores is commonly assumed to be uniform in the theory. We notice that the spatial correlation of some physical quantities [58–60] such as D_{\min}^2 and “softness” only shows a singly exponential decay. A possible reason is that these quantities are defined in terms of nonaffinity or deviation from elasticity. It is interesting to find that the exponential decay in cores does not depend on the strain rates, which can be well fitted by (the dashed-pink line) $\exp(-|\Delta\mathbf{r}|/l_c)$ with a constant correlation length $l_c \approx 2.3 \mu\text{m}$. This rate-independent l_c is well consistent with the unchanged sizes of $C_{\varepsilon_{yz}}(\Delta\mathbf{r})$ cores in Fig. 3, which can be regarded as a measure of the core sizes of STs. The normalized l_c by the particle diameter ($1.55 \mu\text{m}$) is about 1.48, very close to the normalized size (1.1 ± 0.2) of initial rearrangements determined by the spatial correlation of D_{\min}^2 or softness [58]. In the flow of a jammed silicone emulsion, Goyon *et al.* [61] have found a similar flow cooperativity length that is rate independent, and near the jamming point this length is compared with the silicone droplet diameter.

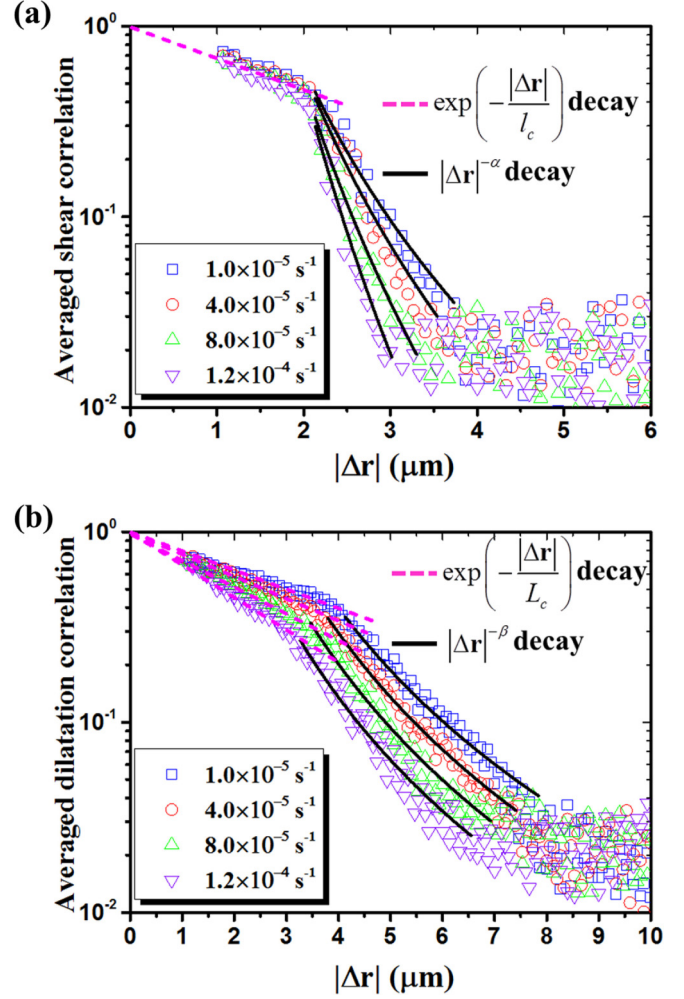


FIG. 5. Angle-averaged elastic correlation vs interparticle distance $|\Delta\mathbf{r}|$: (a) shear $C_{\varepsilon_{yz}}(\Delta\mathbf{r})$ and (b) dilatation $C_{\xi}(\Delta\mathbf{r})$ fields. The dashed-pink lines shown in (a) and (b) are the fits to $\exp(-|\Delta\mathbf{r}|/l_c)$ and $\exp(-|\Delta\mathbf{r}|/L_c)$, respectively. The solid-black lines shown in (a) and (b) are the fits to $|\Delta\mathbf{r}|^{-\alpha}$ and $|\Delta\mathbf{r}|^{-\beta}$, respectively, where $\alpha = 4.5, 5.2, 6.5,$ and 8.0 as the strain rates increase, but $\beta = 3.45 \pm 0.05$ is rate independent.

The power-law decay in $C_{\varepsilon_{yz}}(\Delta\mathbf{r})$ outfields is highly rate dependent, which can be fitted by (the solid-black lines) $|\Delta\mathbf{r}|^{-\alpha}$ with different exponents $\alpha = 4.5, 5.2, 6.5,$ and 8.0 as the strain rates increase. The distance deviated from the power-law decay can be reasonably defined as a characteristic correlation length l_s for the shear full field. It determines that l_s decreases from 3.7 to $3.0 \mu\text{m}$ with increasing $\dot{\gamma}$ from 1.0×10^{-5} to $1.2 \times 10^{-4} \text{ s}^{-1}$. STs interact on each other via nonlocal elastic outfields by themselves. Therefore, l_s *per se* could be understood as the interaction length of STs, that is, the minimum size of avalanches consisting of only two STs. The avalanche sizes decrease with increasing strain rate [56,62]. In athermally sheared Lennard-Jones glasses, Lemaître and Caroli [63] have proposed a scaling law $l_s \propto \dot{\gamma}^{-1/3}$. We find that this scaling law holds well for the currently homogeneous deformation ($\dot{\gamma} < \tau^{-1}$), but gradually deviates due to the shear banding ($\dot{\gamma} > \tau^{-1}$); see Fig. S5 [32].

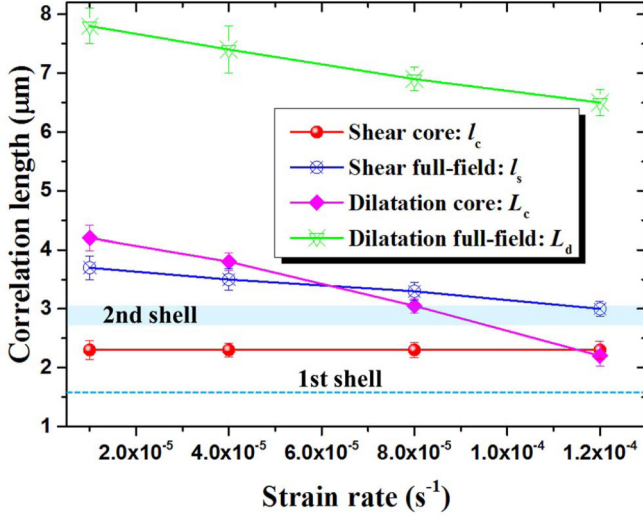


FIG. 6. Correlation lengths of elastic fields as a function of the applied strain rates. The positions of the first- and the second-neighbor shells of the colloidal glass are marked.

Figure 5(b) calculates the averaged correlation of the dilatation field $C_\xi(\Delta\mathbf{r})$, which also shows the two-stage decay with increase of $|\Delta\mathbf{r}|$. The dilatation cores exhibit an exponential decay that can be fitted by (the dashed-pink lines) $\exp(-|\Delta\mathbf{r}|/L_c)$, but with rate-dependent correlation lengths L_c . As the strain rate increases from 1.0×10^{-5} to $1.2 \times 10^{-4} s^{-1}$, L_c decreases from 4.2 to 2.2 μm , corresponding to the size change of the dilatation cores observed in Fig. 4. The dilatation outfields also follow a power-law $|\Delta\mathbf{r}|^{-\beta}$ decay, but with a rate-independent exponent $\beta = 3.45 \pm 0.05$. Again, we define the distance deviated from the power-law decay as a characteristic correlation length L_d of the dilatation full field. The determined L_d values also show negative rate dependence, ranging from 7.8 to 6.5 μm . The length L_d measures the maximum propagation distance of dilatation induced by STs, which is at least twice greater than l_s (3.7 to 3.0 μm). This long-range diffusion behavior possibly arises from STs-enhanced transport of free volume [64], especially in amorphous systems with nondirectional bonding nature [65]. It is noteworthy that either l_s or L_d is much smaller than the sample size of the studied glass. Therefore, these very weakly correlated plateaus at large $|\Delta\mathbf{r}|$ are not noise due to the limits of sample sizes, but possibly result from a certain long-range anomalous decay [66]. In addition, the above spatial correlation analyses and the data repeatability are confirmed by two independent runs performed in the same experimental condition; see Fig. S6 [32].

D. Elastic criterion for shear-banding instability

Figure 6 plots all correlation lengths versus the strain rates, where the positions of the first- and the second-neighbor shells of RDF [see Fig. 1(a)] are marked for better understanding these length scales. The rate-independent correlation length ($l_c \approx 2.3 \mu m$) of the shear cores indicates that STs themselves in the studied glass are localized events at the short-range scale. But, the elastic shear field induced by STs can reach the long-range scale, and its correlation length l_s shows a negative

rate effect. With increasing strain rate, l_s becomes shorter ranged. For example, at the highest $\dot{\gamma} = 1.2 \times 10^{-4} s^{-1}$, l_s decreases into the second shell. The correlation length L_c of the dilatation cores also exhibits a negative rate effect, but more susceptibly than l_s . The values of L_c span a wider range from the long-range (4.2 μm) to short-range (2.2 μm) scale, even below l_c at the highest $\dot{\gamma} = 1.2 \times 10^{-4} s^{-1}$. The correlation length L_d of the dilatation full field always resides in the long-range scale, much larger than other three lengths. From the rate effect of these correlation lengths, the relationship

$$L_c < l_s, \quad (2)$$

which can be identified as an elastic criterion for the shear-banding instability. In other words, the strongly correlated dilatation cores must be confined within the shear-correlation full-fields, whereas the weakly correlated dilatation outfields seem to be trivial. According to the previous study by some of us [29], the dilatation cores actually are the potential regions of activation of STs. Therefore, this criterion $L_c < l_s$ implies that new STs must be activated within the domain of the elastic shear fields of preexisting STs. Only in this way can these adjacent STs strongly interact with each other and ultimately self-organize into a shear band via avalanches.

To visualize this picture directly, we reconstruct the contour plot of local dilatation ξ of particles in a 6- μm -thick y - z section, and trace its spatial evolution in three successive time steps. During this process, the particles participating in STs are superimposed on the contour plots. Here the ST particles are identified by the significant jump of their local strain ε_{yz} and nearest neighbors, as detailed previously [29]. Figure 7(a) gives the typical results of the homogeneous deformation at $\dot{\gamma} = 1.0 \times 10^{-5} s^{-1}$, where the color represents the contour of ξ and white-filled circles denote ST particles. We clearly see that each ST can trace back to its high- ξ source in previous steps. Such spatial correspondences are marked by dashed-line arrows. In the current steps, the STs will relax local dilatation and thus lie in blueish regions. As expected, the high- ξ regions are relatively far from the preexisting ST particles, and their distances are mostly greater than the shear-correlation length l_s (3.7 μm) of STs. In this manner, the new activated ST particles in the next steps have little chance of interacting with STs that occurred in the last steps. Eventually, the accumulation of these independent STs contributes to spatially homogeneous deformation [Figs. 2(a) and 2(b)].

Figure 7(b) presents the inhomogeneous case at $\dot{\gamma} = 1.2 \times 10^{-4} s^{-1}$, where both the contour of ξ and ST particles exhibit a distinct behavior. In the top shear band, we observe that the high- ξ regions induced by STs are always adjacent to the ST particles, and their distances (corresponding to L_c) are indeed shorter than l_s (3.0 μm). The new ST particles in the next steps will be activated at the neighboring high- ξ sites in the last steps. Obviously, these STs are spatiotemporally correlated, which are indicated as three successively generated aligned STs [marked 1–3 in Fig. 7(b)] mediated by DTs along the banding direction. In this situation, STs, both new activated and preexisting, are highly avalanched, due to their overlapped elastic fields. Avalanches of STs finally mature into a shear band that spans the whole system [Figs. 2(c) and 2(d)]. Unfortunately, this full process cannot be captured with the current

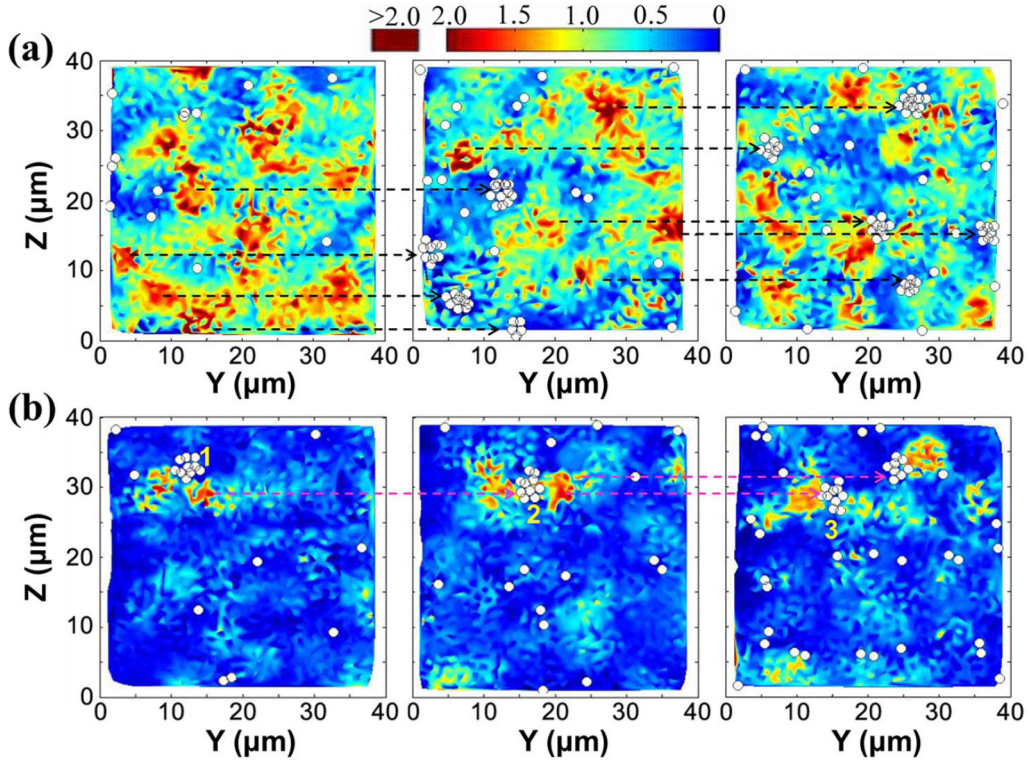


FIG. 7. Typical contour plots of local dilatation ξ of 6- μm -thick y - z sections during three successive time steps, superimposed upon particles participating in STs (white-filled circles). (a) Homogeneous deformation ($\dot{\gamma} = 1.0 \times 10^{-3} \text{ s}^{-1}$) and (b) shear-banding ($\dot{\gamma} = 1.2 \times 10^{-4} \text{ s}^{-1}$) modes. The dashed-line arrows spatially link ST particles with their high- ξ sources.

time resolution (200 s). However, these experimental observations support the atomistic simulations by Şopu *et al.* [12]. They indeed found that maxima of positive volumetric strain just occur in the regions of those self-assembled STs during shear-band initiation. In contrast, the displacement fields between two adjacent STs display rotated vortex structures [14] with relatively low volumetric strain. It is expected that the long-range transport of dilatation or free volume (if $L_c > l_s$) could weaken or even destruct such bridging hard (elastic) vortices, thus rendering STs no longer correlated.

IV. CONCLUSIONS

Our experimental findings substantiate the idea that free-volume dynamics and ST operations are inherently correlated and deeply interdependent [7,29,67,68]. Either local coalescence of free volume or nonlocal shear of STs is only a loose, necessary condition for shear-banding instability in amorphous solids. One must take into account the shear-dilatation causality during STs, which is quantified by $L_c < l_s$. This elastic criterion reveals that only those dilatation- or free-volume confined STs have the chance to interact via their contacted shear fields, and ultimately self-organize into a shear band. This physical picture *coordinates local effect of free volume with nonlocal effect of STs*, thus uniting the two classical mechanisms for shear banding in history.

At last, we argue that the elastic criterion $L_c < l_s$ should be valid in other dilatant shear-banding cases due to the change of structure or temperature, although here it is obtained from the rate effect of shear banding. Our results may be also generalized to a broad range of amorphous solids, where the shear banding results from avalanches of dilatant STs. Importantly, all analyses in this study are based on two very basic quantities: shear strain ε_{ij} and free volume v_f of particles. Both can be defined universally for any amorphous solid, regardless of structural motifs and chemical components. We believe that specific values of the correlation lengths may vary among different systems, but the causality between shear and dilatation of STs should hold well. Nevertheless, some amorphous systems very close to liquid sides may be excluded. This is because that, in such soft systems, the nature of shear banding is not necessary dilatant [48,69,70].

ACKNOWLEDGMENTS

We thank Aneal Lemaître for fruitful discussion. This work was supported by the Basic Science Center for “Multiscale Problems in Nonlinear Mechanics” (Grant No. 11988102) of National Natural Science Foundation of China (NSFC), the NSFC National Outstanding Youth Science Fund Project (Grant No. 12125206), and the NSFC (Grants No. 51971047, No. 11972345, and No. 11790292).

- [1] C. M. Gourlay and A. K. Dahle, *Nature (London)* **445**, 70 (2007).
- [2] P. Schall and M. van Hecke, *Annu. Rev. Fluid Mech.* **42**, 67 (2009).
- [3] A. L. Greer, Y. Q. Cheng, and E. Ma, *Mater. Sci. Eng. R* **74**, 71 (2013).
- [4] T. Divoux, M. A. Fardin, S. Manneville, and S. Lerouge, *Annu. Rev. Fluid Mech.* **48**, 81 (2016).
- [5] M. P. Kroonblawd and L. E. Fried, *Phys. Rev. Lett.* **124**, 206002 (2020).
- [6] N. Yan, Z. Li, Y. Xu, and M. A. Meyers, *Prog. Mater. Sci.* **119**, 100755 (2021).
- [7] A. S. Argon, *Acta Metall.* **27**, 47 (1979).
- [8] P. S. Steif, F. Spaepen, and J. W. Hutchinson, *Acta Metall.* **30**, 447 (1982).
- [9] R. Besseling, L. Isa, P. Ballesta, G. Petekidis, M. E. Cates, and W. C. K. Poon, *Phys. Rev. Lett.* **105**, 268301 (2010).
- [10] D. Klaumünzer, A. Lazarev, R. Maaß, F. H. Dalla Torre, A. Vinogradov, and J. F. Löffler, *Phys. Rev. Lett.* **107**, 185502 (2011).
- [11] V. Chikkadi, D. M. Miedema, M. T. Dang, B. Nienhuis, and P. Schall, *Phys. Rev. Lett.* **113**, 208301 (2014).
- [12] D. Şopu, A. Stukowski, M. Stoica, and S. Scudino, *Phys. Rev. Lett.* **119**, 195503 (2017).
- [13] F. Zeng, M. Q. Jiang, and L. H. Dai, *Proc. R. Soc. London, A* **474**, 20170836 (2018).
- [14] M. Hassani, A. E. Lagogianni, and F. Varnik, *Phys. Rev. Lett.* **123**, 195502 (2019).
- [15] M. Q. Jiang and L. H. Dai, *J. Mech. Phys. Solids* **57**, 1267 (2009).
- [16] O. Reynolds, *Philos. Mag.* **20**, 469 (1885).
- [17] V. Hieronymus-Schmidt, H. Rösner, G. Wilde, and A. Zaccone, *Phys. Rev. B* **95**, 134111 (2017).
- [18] J.-O. Krisponeit, S. Pitikaris, K. E. Avila, S. Küchemann, A. Krüger, and K. Samwer, *Nat. Commun.* **5**, 3616 (2014).
- [19] Y. Shao, K. Yao, M. Li, and X. Liu, *Appl. Phys. Lett.* **103**, 171901 (2013).
- [20] G. Parisi, I. Procaccia, C. Rainone, and M. Singh, *Proc. Natl. Acad. Sci. USA* **5577** (2017).
- [21] T. C. Pekin, J. Ding, C. Gammner, B. Ozdol, C. Ophus, M. Asta, R. O. Ritchie, and A. M. Minor, *Nat. Commun.* **10**, 2445 (2019).
- [22] A. J. Cao, Y. Q. Cheng, and E. Ma, *Acta Mater.* **57**, 5146 (2009).
- [23] K. Karimi, D. Amitrano, and J. Weiss, *Phys. Rev. E* **100**, 012908 (2019).
- [24] R. Dasgupta, H. G. E. Hentschel, and I. Procaccia, *Phys. Rev. Lett.* **109**, 255502 (2012).
- [25] R. Dasgupta, H. G. E. Hentschel, and I. Procaccia, *Phys. Rev. E* **87**, 022810 (2013).
- [26] E. R. Homer and C. A. Schuh, *Acta Mater.* **57**, 2823 (2009).
- [27] M. L. Manning, J. S. Langer, and J. M. Carlson, *Phys. Rev. E* **76**, 056106 (2007).
- [28] A. Le Bouil, A. Amon, S. McNamara, and J. Crassous, *Phys. Rev. Lett.* **112**, 246001 (2014).
- [29] Y. Z. Lu, M. Q. Jiang, X. Lu, Z. X. Qin, Y. J. Huang, and J. Shen, *Phys. Rev. Applied* **9**, 014023 (2018).
- [30] T. Albaret, A. Tanguy, F. Boioli, and D. Rodney, *Phys. Rev. E* **93**, 053002 (2016).
- [31] K. E. Jensen, D. Pennachio, D. Recht, D. A. Weitz, and F. Spaepen, *Soft Matter* **9**, 320 (2013).
- [32] See Supplemental Material at <http://link.aps.org/supplemental/10.1103/PhysRevE.105.045003> for the details of the colloidal glass and the experimental methods, a scaling law for ST avalanche, and the repeatability of experimental data.
- [33] P. Schall, D. A. Weitz, and F. Spaepen, *Science* **318**, 1895 (2007).
- [34] V. Chikkadi, G. Wegdam, D. Bonn, B. Nienhuis, and P. Schall, *Phys. Rev. Lett.* **107**, 198303 (2011).
- [35] A. Ghosh, Z. Budrikis, V. Chikkadi, A. L. Sellaio, S. Zapperi, and P. Schall, *Phys. Rev. Lett.* **118**, 148001 (2017).
- [36] K. E. Jensen, D. A. Weitz, and F. Spaepen, *Phys. Rev. E* **90**, 042305 (2014).
- [37] M. L. Falk and J. S. Langer, *Phys. Rev. E* **57**, 7192 (1998).
- [38] R. Zargar, B. Nienhuis, P. Schall, and D. Bonn, *Phys. Rev. Lett.* **110**, 258301 (2013).
- [39] Y. Rahmani, R. Koopman, D. Denisov, and P. Schall, *Phys. Rev. E* **89**, 012304 (2014).
- [40] Y. Lu, X. Lu, Z. Qin, and J. Shen, *Phys. Rev. E* **94**, 012606 (2016).
- [41] G. Voronoi, *J. Reine Angew. Math.* **134**, 198 (1908).
- [42] D. Klaumünzer, R. Maaß, F. H. Dalla Torre, and J. F. Löffler, *Appl. Phys. Lett.* **96**, 061901 (2010).
- [43] R. Maaß, D. Klaumünzer, and J. F. Löffler, *Acta Mater.* **59**, 3205 (2011).
- [44] R. Maaß, D. Klaumünzer, G. Villard, P. M. Derlet, and J. F. Löffler, *Appl. Phys. Lett.* **100**, 071904 (2012).
- [45] D. Denisov, M. T. Dang, B. Struth, G. Wegdam, and P. Schall, *Sci. Rep.* **3**, 1631 (2013).
- [46] A. Furukawa and H. Tanaka, *Nat. Mater.* **8**, 601 (2009).
- [47] F. Spaepen, *Acta Metall.* **25**, 407 (1977).
- [48] R. Benzi, T. Divoux, C. Barentin, S. Manneville, M. Sbragaglia, and F. Toschi, *Phys. Rev. Lett.* **123**, 248001 (2019).
- [49] P. M. Derlet, H. Bocquet, and R. Maass, *Phys. Rev. Materials* **5**, 125601 (2021).
- [50] S. McNamara, J. Crassous, and A. Amon, *Phys. Rev. E* **94**, 022907 (2016).
- [51] V. Schmidt, H. Rösner, M. Peterlechner, G. Wilde, and P. M. Voyles, *Phys. Rev. Lett.* **115**, 035501 (2015).
- [52] C. Liu, V. Roddatis, P. Kenesei, and R. Maaß, *Acta Mater.* **140**, 206 (2017).
- [53] C. Liu, Y. Ikeda, and R. Maaß, *Scr. Mater.*, **190**, 75 (2021).
- [54] J. D. Eshelby, *Proc. R. Soc. London, A* **241**, 376 (1957).
- [55] J. D. Eshelby, *Proc. R. Soc. London, A* **252**, 561 (1959).
- [56] A. Nicolas, J. Rottler, and J.-L. Barrat, *Eur. Phys. J. E* **37**, 50 (2014).
- [57] J. Chattoraj and A. Lemaître, *Phys. Rev. Lett.* **111**, 066001 (2013).
- [58] E. D. Cubuk *et al.*, *Science* **358**, 1033 (2017).
- [59] D. Wei, J. Yang, M. Q. Jiang, B.-C. Wei, Y.-J. Wang, and L.-H. Dai, *Phys. Rev. B* **99**, 014115 (2019).
- [60] T. Niiyama, M. Wakeda, T. Shimokawa, and S. Ogata, *Phys. Rev. E* **100**, 043002 (2019).
- [61] J. Goyon, and G. O. A. Colin, A. Ajdari, and L. Bocquet, *Nature (London)* **454**, 84 (2008).
- [62] A. Nicolas, E. E. Ferrero, K. Martens, and J.-L. Barrat, *Rev. Mod. Phys.* **90**, 045006 (2018).
- [63] A. Lemaître and C. Caroli, *Phys. Rev. Lett.* **103**, 065501 (2009).
- [64] J. Bokeloh, S. V. Divinski, G. Reglitz, and G. Wilde, *Phys. Rev. Lett.* **107**, 235503 (2011).

- [65] I. Jonas, F. Yang, and A. Meyer, *Phys. Rev. Lett.* **123**, 055502 (2019).
- [66] P. Rissone, E. I. Corwin, and G. Parisi, *Phys. Rev. Lett.* **127**, 038001 (2021).
- [67] M. Q. Jiang, G. Wilde, and L. H. Dai, *Mech. Mater.* **81**, 72 (2015).
- [68] A. Lemaître, *Phys. Rev. Lett.* **89**, 195503 (2002).
- [69] F. Varnik, L. Bocquet, J. L. Barrat, and L. Berthier, *Phys. Rev. Lett.* **90**, 095702 (2003).
- [70] R. Radhakrishnan and S. M. Fielding, *Phys. Rev. Lett.* **117**, 188001 (2016).